University of Nebraska - Lincoln

DigitalCommons@University of Nebraska - Lincoln

2016

Assessing the evolution of soil moisture and vegetation conditions during the 2012 United States flash drought

Jason A. Otkin
University of Wisconsin-Madison, jasono@ssec.wisc.edu

Martha C. Anderson
USDA-ARS, martha.anderson@ars.usda.gov

Christopher R. Hain
University of Maryland at College Park, christopher.hain@nasa.gov

Mark D. Svoboda
University of Nebraska-Lincoln, msvoboda2@unl.edu

David K. Johnson
USDA-ARS, David.Johnson3@ars.usda.gov
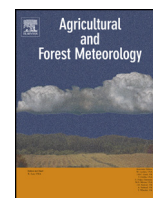
Otkin, Jason A.; Anderson, Martha C.; Hain, Christopher R.; Svoboda, Mark D.; Johnson, David K.; Mueller, Richard; Tadesse, Tsegaye; Wardlow, Brian D.; and Brown, Jesslyn, "Assessing the evolution of soil moisture and vegetation conditions during the 2012 United States flash drought" (2016). *Drought Mitigation Center Faculty Publications*. 99.
https://digitalcommons.unl.edu/droughtfacpub/99

Authors

Jason A. Otkin, Martha C. Anderson, Christopher R. Hain, Mark D. Svoboda, David K. Johnson, Richard Mueller, Tsegaye Tadesse, Brian D. Wardlow, and Jesslyn Brown

Assessing the evolution of soil moisture and vegetation conditions during the 2012 United States flash drought

Jason A. Otkin [a,*], Martha C. Anderson [b], Christopher Hain [c], Mark Svoboda [d], David Johnson [e], Richard Mueller [e], Tsegaye Tadesse [d], Brian Wardlow [d,f], Jesslyn Brown [g]

[a] Cooperative Institute for Meteorological Satellite Studies, University of Wisconsin-Madison, 1225 W. Dayton St., Madison, WI 53706, USA
[b] Agricultural Research Services, United States Department of Agriculture, Hydrology and Remote Sensing Laboratory, Bldg. 007, BARC-West, Beltsville, MD 20705, USA
[c] Earth System Science Interdisciplinary Center, University of Maryland-College Park, 5825 University Research Court, Suite 4001, College Park, MD 20740, USA
[d] National Drought Mitigation Center, School of Natural Resources, University of Nebraska-Lincoln, 819 Hardin Hall, 3310 Holdrege Street, P.O. Box 830988, Lincoln, NE 68583, USA
[e] United States Department of Agriculture, National Agricultural Statistics Service, 1400 Independence Ave. SW, Washington, DC 20250, USA
[f] Center for Advanced Land Management Information Technologies, University of Nebraska-Lincoln, 3310 Holdredge St., Lincoln, NE 68583, USA
[g] U.S. Geological Survey, Earth Resources Observation and Science Center, 47914 252nd Street, Sioux Falls, SD 57198, USA

ARTICLE INFO

ABSTRACT

This study examines the evolution of several model-based and satellite-derived drought metrics sensitive to soil moisture and vegetation conditions during the extreme flash drought event that impacted major agricultural areas across the central U.S. during 2012. Standardized anomalies from the remote sensing based Evaporative Stress Index (ESI) and Vegetation Drought Response Index (VegDRI) and soil moisture anomalies from the North American Land Data Assimilation System (NLDAS) are compared to the United States Drought Monitor (USDM), surface meteorological conditions, and crop and soil moisture data compiled by the National Agricultural Statistics Service (NASS).

Overall, the results show that rapid decreases in the ESI and NLDAS anomalies often preceded drought intensification in the USDM by up to 6 wk depending on the region. Decreases in the ESI tended to occur up to several weeks before deteriorations were observed in the crop condition datasets. The NLDAS soil moisture anomalies were similar to those depicted in the NASS soil moisture datasets; however, some differences were noted in how each model responded to the changing drought conditions. The VegDRI anomalies tracked the evolution of the USDM drought depiction in regions with slow drought development, but lagged the USDM and other drought indicators when conditions were changing rapidly. Comparison to the crop condition datasets revealed that soybean conditions were most similar to ESI anomalies computed over short time periods (2–4 wk), whereas corn conditions were more closely related to longer-range (8–12 wk) ESI anomalies. Crop yield departures were consistent with the drought severity depicted by the ESI and to a lesser extent by the NLDAS and VegDRI datasets.

© 2015 Elsevier B.V. All rights reserved.

1. Introduction

The 2012 drought that impacted major agricultural areas across the central U.S. was the worst drought to affect this region since 1988 and had similar magnitude and spatial extent to the severe droughts that occurred during the 1930s and 1950s (Hoerling et al., 2014). The almost complete absence of heavy rainfall events during the growing season, combined with record high temperatures, strong winds, and abundant sunshine, led to rapid decreases in soil moisture content and the rapid emergence of flash drought conditions (Lydolph, 1964; Mozny et al., 2012; Otkin et al., 2013; Mo and Lettenmeier, 2015). According to the U.S. Drought Monitor (USDM; Svoboda et al., 2002), drought coverage and intensity rapidly increased during June and July in response to the anomalous weather conditions, with nearly 80% of the contiguous U.S. characterized by at least abnormally dry conditions by the end of summer. Most of the central U.S., including the Corn Belt, experienced severe drought (or worse) conditions at some point during the growing season (Mallya et al., 2013). Recent modeling studies have shown that this exceptional drought event was not forced by tropical sea

surface temperature anomalies. Instead, it was associated with natural variations in the weather that led to the development of a persistent upper-tropospheric ridge that inhibited convection and caused exceptionally warm temperatures to occur across the region for several months (Kumar et al., 2013; Wang et al., 2014; Hoerling et al., 2014; Diffenbaugh and Sherer, 2013).

The 2012 drought was one of the most expensive natural disasters in U.S. history with Federal crop indemnity payments alone exceeding $17 billion (USDA, 2013). Crop losses were especially large because the most severe drought conditions occurred during critical stages of crop development, such as pollination in corn and the grain filling stage in soybeans. Prior work has shown that even short periods (e.g. several days) of intense water stress can result in large crop yield reductions (e.g. Meyer et al., 1993; Saini and Westgate, 1999; Calvino et al., 2003; Earl and Davis, 2003; Barnabás et al., 2008; Mishra and Cherkauer, 2010; Prasad et al., 2011; Kebede et al., 2012; Hunt et al., 2014). In 2012, however, severe moisture and heat stress lasted for more than a month across most major agricultural areas of the country, thereby leading to the lowest corn yields since 1995. If long-term yield trends are accounted for, the percentage yield loss was one of the largest on record going back to 1866 (Hoerling et al., 2014; Boyer et al., 2013). The large yield loss is consistent with a recent study by Lobell et al. (2014) that assessed yield trends during recent decades for different levels of moisture stress. Their analysis showed that yield gains have been smallest on a percentage basis for growing seasons in which large vapor pressure deficits indicative of severe drought conditions occur during critical crop yield development stages. As drought conditions spread westward during the summer, ranchers also experienced substantial impacts through a combination of higher feed prices, a lack of high quality forage, and heat-related animal stress, with many ranchers forced to either sell or relocate their livestock to other parts of the country (USDA, 2012). The rapid onset of severe drought conditions meant that farmers and ranchers had little time to prepare for its adverse effects. It is possible, however, that greater use of drought indicators that respond quickly to changing conditions, such as the satellite-derived Evaporative Stress Index (ESI; Anderson et al., 2007a,b), may promote drought mitigation efforts during future flash drought events by providing earlier warning of drought development (Otkin et al., 2014, 2015a,b).

High-resolution estimates of soil moisture and vegetation health conditions are necessary to accurately assess the severity and geographic extent of drought conditions at spatial and temporal scales sufficient for stakeholders to make informed management decisions. Moreover, an accurate assessment of current conditions is a prerequisite for producing useful drought intensification forecasts over monthly to seasonal time scales. In this paper, the evolution of several drought indicators sensitive to vegetation health and soil moisture conditions will be examined during the onset and development of the 2012 flash drought. These indicators include the ESI, which uses satellite thermal infrared observations and a land surface energy balance model to estimate anomalies in evapotranspiration (ET) and the Vegetation Drought Response Index (VegDRI; Brown et al., 2008) that uses satellite, land, and climate observations to assess vegetation health conditions. The evolution of the satellite-derived datasets will be compared to modeled soil moisture anomalies from the North American Land Data Assimilation System (NLDAS; Xia et al., 2012a,b, 2014) and to time series of precipitation and meteorological conditions. The accuracy of these datasets will be assessed for different locations and time periods through comparison with USDM drought analyses and county-level crop and range condition datasets compiled by the United States Department of Agriculture (USDA) National Agricultural Statistics Service (NASS). Though the NASS datasets are qualitative, they provide very valuable ground truth of the actual impact of the drought on agriculture. Each of these datasets is described in Section 2. The overall evolution of the drought and relationships between the drought indicators and crop conditions and yield are assessed in Section 3, with conclusions presented in Section 4.

2. Data and methodology

2.1. Evaporative Stress Index

The ESI depicts standardized anomalies in ET fraction (ET/ET_{ref}), where ET is the actual ET flux retrieved under clear-sky conditions and ET_{ref} is a reference ET flux based on a Penman-Monteith formulation (Allen et al., 1998). Reference ET is used in this equation to minimize the impact of non-moisture related drivers of ET, such as the seasonal cycle in solar radiation, when assessing anomalies in ET. Similarly, the use of clear-sky ET minimizes impacts of cloud cover on ET variability, again focusing on soil moisture drivers. The Atmosphere-Land Exchange Inverse (ALEXI) model (Anderson et al., 1997, 2007a, 2011) is used to estimate the actual ET flux. ALEXI uses a two-source energy balance model (Norman et al., 1995) and land surface temperature (LST) retrievals obtained from satellite thermal infrared imagery to compute sensible, latent, and ground heat fluxes for vegetated and bare soil components of the land surface. The partitioning of the surface energy fluxes is accomplished using vegetation cover fraction estimates derived from the MODIS leaf area index product (Myneni et al., 2002). The total surface energy budget is computed using the observed increase in LST from ~1.5 h after local sunrise until 1.5 h before local noon, with closure of the energy balance equations achieved using the McNaughton and Spriggs (1986) atmospheric boundary layer growth model. Lower-tropospheric temperature profiles used by the boundary layer model are obtained from the Climate Forecast System Reanalysis dataset (Saha et al., 2010). The ALEXI model is run each day over the contiguous U.S. (CONUS) with 4-km horizontal grid spacing using LST retrievals and insolation estimates derived from the Geostationary Operational Environmental Satellite (GOES) imager.

While the ESI ideally includes only clear-sky retrievals of ET, incomplete cloud screening of the thermal infrared-derived LST inputs can add noise to the ET time series used in the index computation. These errors are reduced using a temporal smoothing algorithm that identifies days with ET estimates that differ by more than one standard deviation from surrounding days within a 14 day moving window. Anderson et al. (2013) have shown that this method effectively removes cloud-contaminated ET estimates because abrupt changes in daily ET are more likely to occur because of cloud effects on surface heating than to rapid changes in soil moisture content. The remaining clear-sky ET estimates are then composited over longer time periods to achieve more complete domain coverage.

Standardized ET fraction anomalies, expressed as pseudo *z*-scores normalized to a mean of 0 and a standard deviation of 1, are computed each week using 2, 4, 8, and 12 wk composite periods. The mean ET fraction and standard deviations for each composite period are computed at each grid point in the CONUS domain using data from 2001 to 2014. Standardized anomalies are computed as:

$$\text{ESI}(w, y) = \frac{\langle v(w, y) \rangle - (1/ny) \sum \langle v(w, y) \rangle}{\sigma(\omega)} \tag{1}$$

where the first term in the numerator is the composite ET fraction for week *w* and year *y* at a given grid point, the second term is the mean ET fraction for week *w* averaged over all years, and the denominator is the standard deviation. By standardizing the anomalies, this means that negative (positive) values depict below (above) average ET fluxes, which are typically associated with lower (higher) than average soil moisture content and poorer (better)

than average vegetation health in the absence of other stressors such as disease.

2.2. Vegetation Drought Response Index

VegDRI is an empirical method that combines satellite observations of vegetation health with climate data and other information about the land surface to identify regions containing drought stressed vegetation. Two climate-based drought indices, including the Standardized Precipitation Index (SPI; McKee et al., 1993) computed over a 36-wk time period and the self-calibrated Palmer Drought Severity Index (Wells et al., 2004) are used by VegDRI. Normalized difference vegetation index data from the Advanced Very High Resolution Radiometer are used to calculate seasonal greenness and start of season metrics input into VegDRI. Several static biophysical variables describing environmental characteristics that influence drought stress on vegetation, such as land use/land cover, soil available water holding capacity, ecoregion type, and irrigation, are also included in the model. A classification and regression tree analysis is then applied to the historical information in the database to empirically derive VegDRI analyses each week. VegDRI output is typically displayed as discrete categories; however, because the underlying data are continuous, they were converted into standardized anomalies using data from 2000 to 2012 to ease comparison with other datasets used in this study. VegDRI data at 1-km native resolution were aggregated to the 4-km ESI grid. A complete description of the VegDRI model can be found in Brown et al. (2008) and Tadesse et al. (2015).

2.3. North American Land Data Assimilation System

Modeled soil moisture anomalies were computed using data from several NLDAS models (Xia et al., 2012a,b), including the Noah (Ek et al., 2003; Barlage et al., 2010; Wei et al., 2013), Mosaic (Koster and Suarez, 1996), and Variable Infiltration Capacity (VIC; Liang et al., 1996) models. Each land surface model simulates soil moisture content in multiple layers using energy and water balance equations. Because the models differ in their treatment of key processes such as evaporation, drainage, vegetation rooting depth, and canopy uptake, their soil moisture responses can differ due to local climate, soil, and vegetation characteristics. Daily soil moisture values from each model and the ensemble mean of all models (hereafter referred to as NMV_AVE) were interpolated from the 0.125° resolution NLDAS grid to the 4-km ESI grid using a nearest neighbor approach. Soil moisture data in the topsoil (0–10 cm) and total column (0–200 cm) layers were averaged over 2- and 4-wk periods, with standardized anomalies for each soil layer (hereafter referred to as TS and TC, respectively) computed at weekly intervals using data from 1979 to 2014. The soil moisture response of each model will be compared to the ensemble mean and to the other drought indicators.

2.4. North American Regional Reanalysis

The evolution of the near-surface atmospheric conditions was evaluated using NARR data (Mesinger et al., 2006). Daily averages were computed for 10-m wind speed, 2-m temperature, and 2-m dew point depression using analyses available every 3 h on a 32-km resolution grid. The daily averages were then interpolated to the ESI grid using a nearest neighbor approach, with standardized anomalies for 1-wk periods computed at weekly intervals using data from 2000 to 2014.

2.5. Precipitation datasets

Gridded daily precipitation for 1948–2014 obtained from the Climate Prediction Center's (CPC) 0.25° resolution precipitation analysis (Higgins et al., 2000) was interpolated to the ESI grid using a nearest neighbor approach and then summed at weekly intervals to create 1-, 4-, 8-, and 12-wk accumulated precipitation amounts. SPI values for 4-, 8-, and 12-wk periods were subsequently computed. The SPI is a standardized variable widely used to identify meteorological drought conditions, with values less (greater) than zero indicating the observed precipitation was less (more) than the climatological median precipitation for a given length of time and time of year.

2.6. United States Drought Monitor

The USDM is a widely used drought analysis generated each week through expert synthesis of multiple data sources, including precipitation and soil moisture anomalies, surface stream flow departures, various drought metrics, crop and range conditions, and impact reports from local observers. Because it conveys drought information at multiple time scales and for a wide range of impacts (including socioeconomic), the USDM should not be considered an absolute measure of drought severity. By using a variety of data sources, most with high spatial resolution (sub-county), the USDM can depict both large-scale and localized areas of drought. For this study, weekly USDM analyses in shape file format were interpolated to the 4-km ALEXI grid by assigning numerical values to each drought category, with abnormally dry (D0) = 0, moderate drought (D1) = 1, severe drought (D2) = 2, extreme drought (D3) = 3, and exceptional drought (D4) = 4. When no drought conditions were present the value was set to −1.

2.7. USDA crop and soil moisture datasets

The USDA NASS produces publically available state-level soil moisture and crop condition estimates each week from April-November based on survey data collected from ∼4000 local experts knowledgeable in visually identifying crop status and soil moisture conditions. For this study, the author signed a confidentiality agreement with the USDA NASS to access county-level crop condition and soil moisture datasets, where the data were spatially smoothed to ensure that no individual records or confidential data were publically released. Health condition estimates ranging from very poor to excellent are reported for pasture and range and for all major agricultural crops, including corn, soybeans, cotton, winter wheat, spring wheat, peanuts, barley, oats, and sorghum. In addition, categorical topsoil and subsoil moisture assessments ranging from very short to surplus are made each week, with the former (latter) category indicating that the soil moisture content is much less (greater) than that required for normal crop development. Numerical values were then assigned to each crop condition (very poor, poor, fair, good, and excellent) and soil moisture (very short, short, adequate, and surplus) category, with average crop conditions computed for each county using all reports available during a given week. These county level datasets were spatially smoothed using a 3×3 grid point square moving window after first being interpolated to the 4-km ESI grid. Crop and soil moisture anomalies were computed each week by subtracting the mean conditions from the 2002 to 2014 period of record.

The impact of the drought conditions on the end-of-season crop yield was also assessed using county level yield statistics compiled by NASS. Corn, soybean, winter wheat, and spring wheat yields from 2000 to 2014 were obtained from the NASS Quick Stats database (http://quickstats.nass.usda.gov). A least squares regression line was fit to the annual yield time series for each

county and crop to account for local changes in yield over time, and then trend-adjusted yield departures were computed for each year.

3. Results

3.1. Large-scale drought analysis

This section examines the overall evolution of conditions across the U.S. during the 2012 drought event from drought onset during late spring through drought maturation during the summer and the northwestward progression of the core drought area during the fall. Figs. 1 and 2 show the evolution of the USDM, SPI_8WK, NMV_AVE topsoil moisture, NASS topsoil moisture and crop condition, ESI_4WK, and VegDRI datasets at monthly intervals from 07 April to 28 October. The time period lengths for each variable were chosen to minimize differences in their response time to the anomalous conditions. For example, compared to the 8-wk SPI, a shorter 4-wk time period was used to compute the ESI and NMV_AVE anomalies because vegetation and soil moisture tend to respond to rainfall anomalies occurring over longer time periods. The VegDRI data, however, will represent drought on a slightly longer time scale due to its use of long-term climate variables such as the 36-wk SPI.

On 07 April, drought conditions were present across the southwestern and north-central U.S. and along the East Coast, with the worst conditions located in Georgia and west Texas according to the USDM. Overall, these drought areas were well captured by the NMV_AVE and ESI_4WK anomalies; however, there were some differences in their spatial extent and magnitude. For example, negative ESI_4WK anomalies cover a much larger area of the northern U.S. These negative ET anomalies developed in response to a prolonged period of record heat during March (Blunden and Arndt, 2013) and indicate that the newly emerged vegetation became moisture stressed because their shallow roots were unable to access sufficient subsoil moisture once the top few cm of the soil profile became dry. Thus, the ESI_4WK anomalies across this part of the country are indicative of short-term dryness at this time. Their large spatial extent, however, is consistent with the widespread negative topsoil moisture anomalies reported in the NASS dataset. The VegDRI analysis also depicts drought in many parts of the country, including the southwestern and southeastern U.S.; however, it does not depict drought over New Mexico and Texas or over New England because the vegetation signal is considered too weak at this time of the year.

By 28 April, dry conditions were becoming more widespread across the eastern U.S. according to the SPI_8WK, NMV_AVE, and NASS soil moisture datasets; however, only minor changes were made to the USDM analysis. The ESI_4WK dataset contains a large area of positive anomalies across the south-central U.S. within a region of above average rainfall. These anomalies indicate that the vegetation was growing rapidly in response to the favorable conditions, which is supported by the positive NASS crop condition anomalies. The VegDRI dataset also contains positive anomalies across this part of the country; however, they are smaller than the ESI_4WK anomalies. Across the north central U.S., the ESI_4WK anomalies had become less extreme, possibly because the vegetation had developed a deeper root structure that could access more soil moisture and support higher ET rates. Farther to the east, large precipitation deficits from Pennsylvania to southern New England led to the development of large topsoil moisture anomalies in the NMV_AVE dataset. The ESI_4WK anomalies were near normal except for areas along the Atlantic Coast, whereas the VegDRI anomalies were mostly positive across the region.

By 02 June, large negative SPI_8WK anomalies had developed across most of the southern U.S., with especially large rainfall deficits located in the south central U.S. The rapid transition from positive to negative anomalies is also evident in the ESI_4WK and NMV_AVE datasets, which now contain large negative anomalies across most of the central U.S. The NASS datasets indicate that the topsoil moisture content and to a lesser extent the crop conditions were below average across most of the central U.S. The worst soil moisture conditions were located in the mid-Mississippi River valley where some areas experienced up to a 2-category increase in drought severity during the previous five weeks according to the USDM. Unlike the other datasets, the VegDRI anomalies mostly remained positive or only became slightly negative across the central U.S. The delayed response of this metric to the rapidly worsening conditions likely results from its use of long-term climate variables such as the 36-wk SPI that change more slowly than fast response drought indicators such as the ESI.

Conditions continued to rapidly deteriorate across most of the central U.S. during June in response to the onset of very hot temperatures and the continuation of well below normal rainfall. By 30 June, large negative NASS topsoil moisture anomalies extended from the central Rockies eastward across the entire Corn Belt. Crop and range conditions were also beginning to rapidly deteriorate as the vegetation was increasingly unable to cope with the adverse weather and soil moisture conditions. Overall, the ESI_4WK and NMV_AVE datasets accurately represent the spatial extent of the drought; however, both depict more severe drought than the USDM in several locations. This is consistent with prior work (e.g. Otkin et al., 2013) that has shown that the USDM tends to respond too slowly to rapidly changing conditions. Both datasets indicate that extreme drought had developed within regions characterized by especially large rainfall deficits along the mid-Mississippi River valley. The VegDRI anomalies have also decreased within this region, but remain too small compared to the other datasets. VegDRI performance is better in the western U.S. where it depicts widespread severe drought conditions.

After enduring the hottest July on record and receiving below normal rainfall (Diffenbaugh and Sherer, 2013), extreme to exceptional drought conditions (D3-D4 in the USDM) encompassed most of the central U.S. by the beginning of August (Fig. 2). According to the USDM, more than 80% of the U.S. was characterized by at least abnormally dry conditions at the peak of the drought on 24 July (not shown). Many locations had experienced flash drought during the previous two months as conditions rapidly transitioned from being drought free to the two worst (D3 and D4) drought categories in the USDM. Very large negative NMV_AVE and ESI_4WK anomalies were present within the core drought regions characterized by the largest SPI_8WK anomalies. The spatial extent and magnitude of these anomalies are consistent with the very poor crop conditions present across most of the central U.S. Though the VegDRI anomalies had also decreased across this part of the country, their magnitude was still much smaller than the other drought indicators.

Several episodes of beneficial rainfall during August led to some improvements to the drought depiction by 01 September along the eastern periphery of the core drought region from Arkansas to Michigan. The wetter conditions in the east combined with the continuation of hot, dry weather in the west led to a westward shift of the core drought region to the central High Plains. Although the NASS topsoil moisture conditions had improved slightly within the eastern Corn Belt, the crops were so badly damaged by this time that only minor gains are evident in the crop condition and ESI_4WK datasets. The VegDRI anomalies accurately captured the spatial extent of the severe drought conditions from the Rocky Mountains eastward to the Mississippi River valley. Further to the west, unusually heavy rainfall across the Desert Southwest led to very large positive ESI_4WK anomalies indicative of much higher than normal ET rates. Some improvements were also evident in the
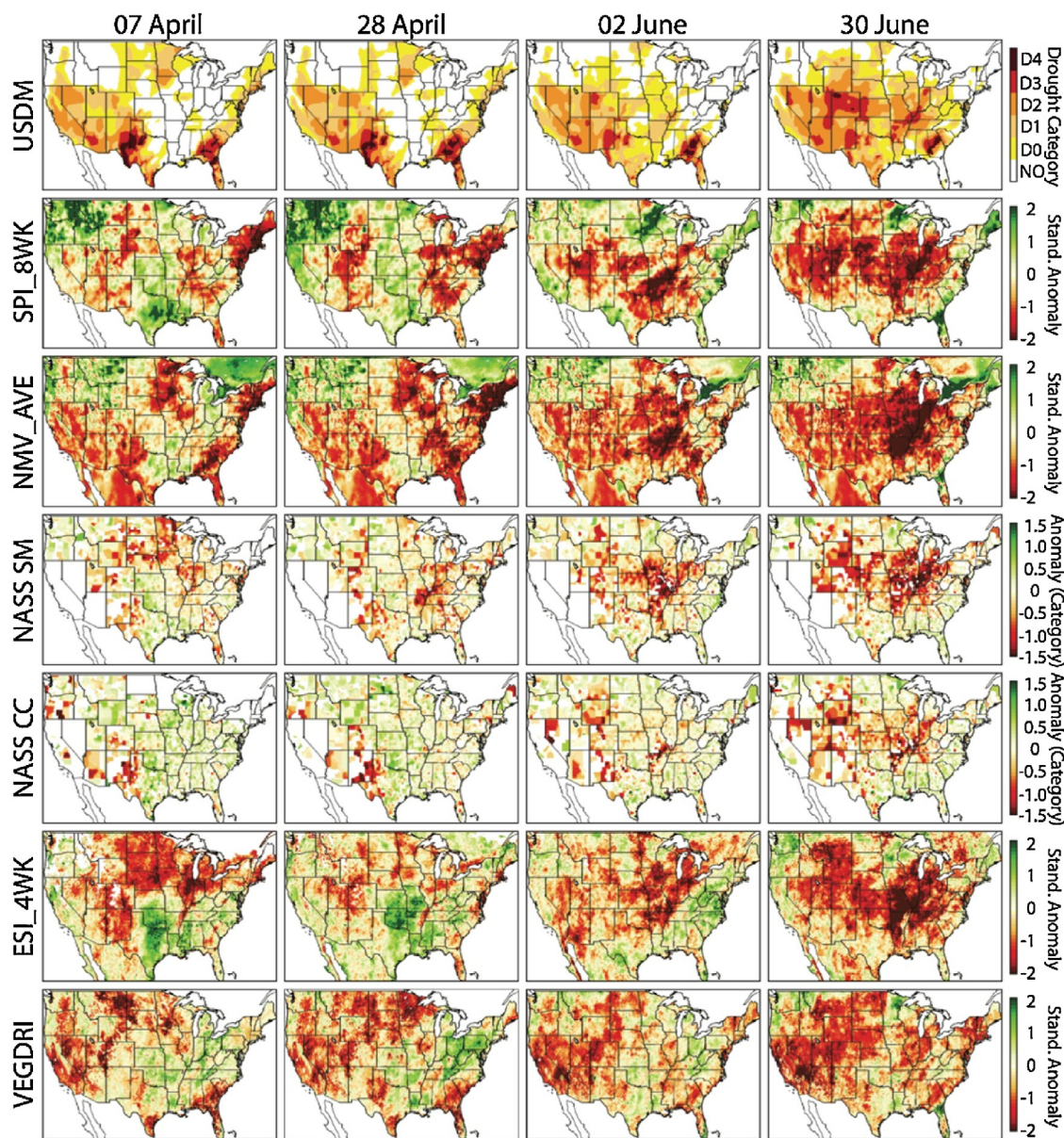
Fig. 1. Temporal evolution of the United States Drought Monitor (USDM) drought depiction, and 8-wk Standardized Precipitation Index (SPI), 4-wk modeled total column soil moisture (NMV_AVE), National Agricultural Statistics Service (NASS) topsoil moisture and crop condition, 4-wk Evaporative Stress Index (ESI), and Vegetation Drought Response Index (VegDRI) anomalies from 07 April until 30 June 2012.

VegDRI data and to a lesser extent in the NMV_AVE topsoil moisture anomalies. The USDM drought depiction improved by one category in most places, but remained high to reflect the impact of long-term dryness across the region.

By 29 September, very dry conditions had developed from the Pacific Northwest to the Upper Midwest, with SPI_8WK anomalies <−2 in many locations. These large rainfall departures combined with warmer than average temperatures led to a northward expansion of drought conditions into the north central U.S. and further intensification of the extreme drought over the central High Plains. The worsening drought conditions are evidenced by the increased spatial extent of large negative anomalies in the ESI_4WK, NMV_AVE, and VegDRI datasets across the north central U.S. and a concurrent increase in large negative NASS topsoil moisture and crop condition anomalies across this region.

Finally, by the end of October, the core drought area had become entrenched over the central High Plains from the Texas panhandle northward to western South Dakota. Very dry conditions are

evident in each dataset across this part of the country. Continued wet weather across the eastern U.S., however, led to further improvements to the USDM drought depiction along the Mississippi River valley. The ESI_4WK anomalies capture the improving conditions in the eastern U.S. as indicated by the return to normal or above normal crop condition and soil moisture anomalies in the NASS datasets. Though not as large, improvements were also evident in the VegDRI and NMV_AVE datasets.

3.2. Regional drought analysis

In this section, the drought evolution will be examined more closely for locations that experienced severe drought conditions during different parts of the growing season and are characterized by different climate regimes and agricultural interests. Unlike the previous section, anomaly time series will be shown at weekly intervals for each variable and will be assessed separately for each crop type and NLDAS model, and for anomalies computed over
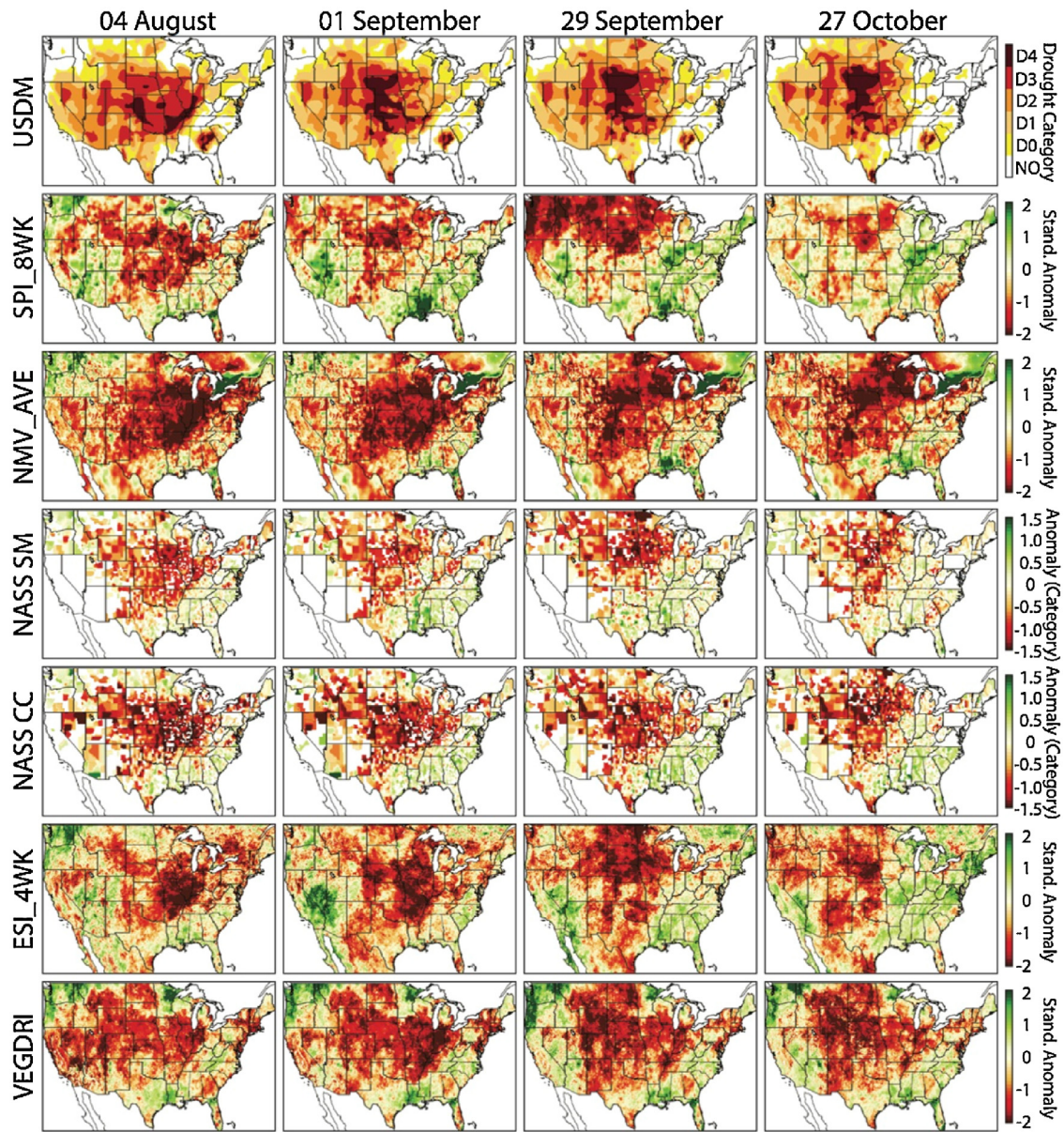
Fig. 2. Same as Fig. 1 except from 04 August until 27 October 2012.

different time periods. The data will be displayed using a visualization method developed in prior studies (e.g. Otkin et al., 2013) as shown in Fig. 3. The USDM is displayed in the first column, with weekly rainfall totals and 1-wk anomalies in surface temperature, dew point depression, and wind speed shown in the next three columns. SPI values for 4- and 12-wk periods are shown next, followed by anomalies in the NASS topsoil moisture, subsoil moisture, range, corn, soybeans, and winter wheat conditions. After that, anomalies are shown for VegDRI and for the ESI computed over 2-, 4-, 8-, and 12-wk periods. The last sixteen columns show anomalies in topsoil and total column soil moisture content computed over 2- and 4-wk periods for the Noah, Mosaic, and VIC models and also for their ensemble mean.

3.2.1. West-central Missouri

Fig. 3 shows weekly values for each variable averaged using all grid points in west-central Missouri (CPC climate division 3). At the beginning of March, abnormally dry conditions were present across the region as signified by negative anomalies in most datasets. This

dryness was partially alleviated by several heavy rainfall events from the end of March to the first week of May that led to large positive SPI and ESI anomalies at all time scales. The positive ESI anomalies indicate that the ET had greatly increased in response to the heavy rainfall and warm temperatures, which is consistent with the above average range and winter wheat conditions in the NASS dataset. Though improvements were also evident in the VegDRI and NLDAS datasets, these changes were modest and most of the anomalies remained negative even though short-term conditions had improved.

After receiving beneficial rainfall during the spring, very dry weather returned to the region during May and coincided with a prolonged hot and windy spell that caused soil moisture and crop conditions to rapidly deteriorate. Temporal changes in the short-range ESI anomalies (2–8 wk) were exceptionally large at the beginning of the flash drought event and closely mirrored the observed crop condition changes. The VegDRI and 12-wk ESI anomalies also decreased, but at a slower rate than the shorter-range ESI anomalies. Each of the NLDAS models also exhibited rapid
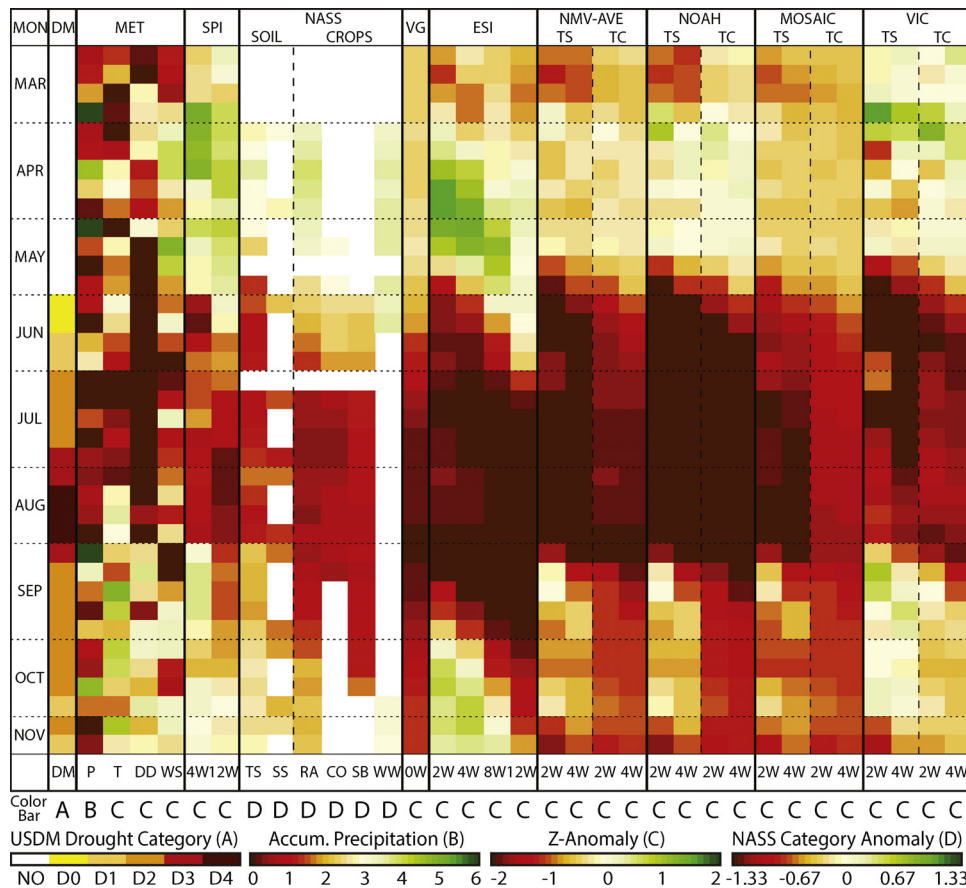
Fig. 3. Drought evolution across west-central Missouri during 2012. The weekly USDM drought category is shown in column 1. The weekly rainfall (cm) is shown in column 2, with z-anomalies for 1-wk average surface temperature, dew point depression, and wind speed shown in columns 3–5. Note that the z-anomaly color bar is reversed for each of these variables so that positive anomalies indicative of enhanced drying are shown in red and brown colors. The SPI values for 4 and 12 wk time periods are shown in columns 6–7. NASS topsoil and subsoil moisture anomalies are shown in columns 8–9, with crop condition anomalies for range, corn, soybeans, and winter wheat shown in columns 10–13. Standardized VegDRI anomalies are shown in column 14. ESI z-anomalies for 2, 4, 8, and 12 wk composite periods are shown in columns 15–18, with 2- and 4-wk z-anomalies for topsoil (0–10 cm) and total column (0–2 m) soil moisture for the NMV ensemble average and for the Noah, Mosaic, and VIC models shown in columns 19–22, 23–26, 27–30, and 31–34, respectively. (For interpretation of the references to color in this figure legend, the reader is referred to the web version of this article.)

decreases in soil moisture at the end of May that were consistent with changes in the NASS soil moisture dataset and preceded their appearance in the ESI by one week. These changes first appeared in the TS moisture and shorter 2-wk composites before appearing in the TC and 4-wk soil moisture anomalies. As drought conditions intensified during the summer, most of the drought indicators continued to deteriorate except for the VIC soil moisture anomalies, which were more sensitive to small rainfall events. The USDM drought severity lagged the other drought metrics by several weeks during the entire event.

Heavy rainfall at the beginning of September led to rapid improvements in the TS and TC moisture in all of the NLDAS models and the reappearance of positive 4-wk SPI values. The ESI anomalies, however, remained at or near their lowest values for the year, and did not exhibit substantial improvements until several weeks later. This behavior indicates that the vegetation was initially dormant or so badly damaged that it could not immediately respond to the improving conditions. It took a prolonged period of cool, wet conditions before the vegetation could recover enough to transpire at higher than normal rates during October. The initial lack of improvement in the ESI is consistent with trends in the NASS crop condition datasets. The 2-category improvement in the USDM at the beginning of September was more representative of the above normal rainfall than it was of improving vegetation conditions. The VegDRI anomalies reached their lowest values during the peak of the drought at the end of August and then slowly recovered during

the fall. Consistent with its use of long-term climate variables, its evolution more closely matched the NLDAS ensemble model average TC soil moisture anomalies during the drought event; however, differences were larger with respect to the individual models.

3.2.2. South-central Wisconsin

This section describes the evolution of the drought over south-central Wisconsin (CPC climate division 8). Inspection of Fig. 4 shows that record warmth during March led to negative anomalies in most datasets despite the slightly above normal rainfall. The spread in the NLDAS soil moisture anomalies was very large at this time. TS moisture anomalies were positive in the VIC model, but negative in the Noah and Mosaic models, whereas the TC moisture anomalies were positive in the Noah model but negative in the other models. Large model differences are also evident later in the spring during a period of moderate rainfall that greatly improved TS moisture conditions, especially in the Noah and VIC models, but led to only minor improvements in the TC soil moisture. The short-range ESI anomalies became slightly positive during May in response to the improved TS moisture conditions. The negative VegDRI anomalies present at the beginning of March continued to increase during the spring due to long-term dryness across the region.

Extreme weather conditions characterized by well below normal rainfall, record high temperatures, large dew point depressions, and unusually strong winds developed across the region during
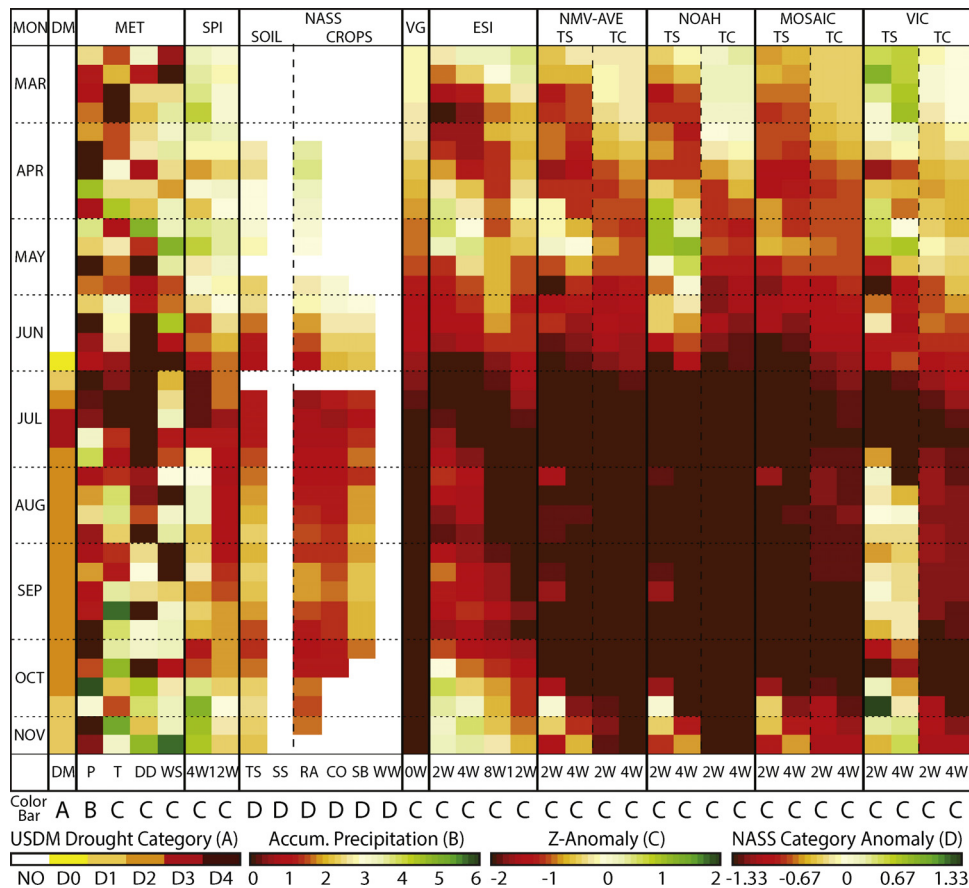
Fig. 4. Same as Fig. 3, except for south central Wisconsin. (For interpretation of the references to color in this figure legend, the reader is referred to the web version of this article.)

June and the first half of July. Vegetation conditions as indicted by the ESI and NASS datasets rapidly deteriorated during this time period because of the increased evaporative demand and the already short soil moisture conditions. Pasture and range conditions were the first to deteriorate, followed in subsequent weeks by decreases in corn and soybean conditions. Almost all of the satellite and model-based drought indicators depicted extreme drought conditions by the beginning of July. Though the USDM drought severity increased an impressive four categories in four weeks during this flash drought, its period of rapid intensification was delayed by up to four weeks compared to the other datasets, especially those computed over 2- and 4-wk time periods. The earlier onset of the large negative anomalies in the ESI and modeled soil moisture datasets, however, is consistent with the large negative anomalies in the NASS datasets.

Heavy rainfall during the last two weeks of July allowed conditions to improve slightly, with the 4-wk SPI returning to normal. Large differences are again evident in the NLDAS datasets, with the VIC model showing much larger improvements, especially in TS moisture, that lasted throughout the late summer and fall recovery period. Given that each of these models had similar anomalies preceding the first rainfall, their different responses are likely due to differences in their infiltration and runoff rates. Compared to the NASS TS moisture dataset, the VIC model is likely too wet, whereas the Noah and Mosaic models are too dry. The VegDRI anomalies became very large in July and then remained strongly negative during the rest of the growing season even as conditions were slowly improving in the other datasets. The delayed VegDRI response was likely due to its use of the 36-wk SPI because this variable remained strongly negative during this time period. The ESI

anomalies displayed different behavior depending on the composite period length, with the short-term composites showing minor improvements after the first rainfall, whereas the long-range composites did not improve until September. Overall, changes in corn conditions were closely related to the long-range (8- and 12-wk) ESI anomalies, whereas the soybean conditions tracked changes in the shorter 2- and 4-wk anomalies. This behavior is consistent with prior work by Peng et al. (2014) using other vegetation indices.

3.2.3. Northwestern Kansas

The evolution of the drought conditions over northwestern Kansas (CPC climate division 1) is shown in Fig. 5. At the beginning of March, most datasets indicated near to slightly drier than normal conditions. Beneficial rainfall starting at the end of March led to positive SPI anomalies and above normal soil moisture and crop conditions according to the NASS datasets. Though there are some differences in magnitude, the evolution of the modeled TS and TC moisture anomalies are similar in each NLDAS model. The ESI anomalies remained negative longer than the other datasets during the first part of April presumably because the vegetation had not yet emerged or was still too small to take full advantage of the increased soil moisture content. The VegDRI anomalies were near zero initially before slowly increasing as spring transitioned into summer.

Drought conditions began to rapidly intensify during May and June in response to a prolonged period of hot, windy, and dry weather that quickly depleted the TS moisture according to the NASS dataset and each of the NLDAS models. Rapid decreases initially occurred in the NLDAS TS anomalies before becoming evident in the ESI anomalies two weeks later and the VegDRI dataset after
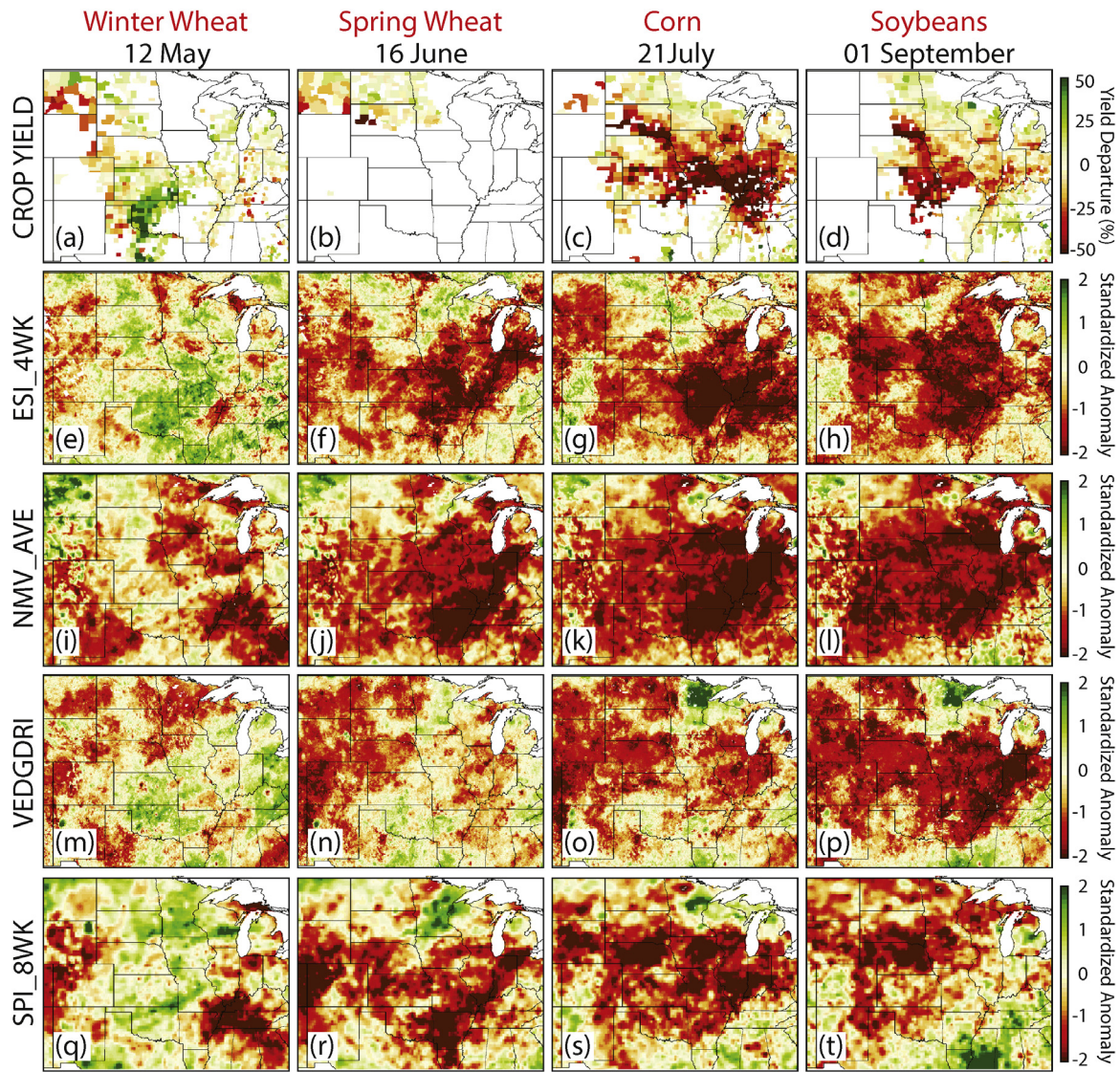
Fig. 5. Same as Fig. 3, except for northwestern Kansas. (For interpretation of the references to color in this figure legend, the reader is referred to the web version of this article.)

that. Periodic small rainfall events starting in July led to minor improvements in the 2- and 4-wk ESI composites and the NLDAS TS moisture anomalies; however, the longer-range ESI composites and NLDAS TC moisture anomalies continued to decrease during the summer as long-term rainfall deficits continued to accumulate. The negative soil moisture anomalies were largest for the Noah model and smallest for the VIC model, similar to the results described in previous sections. The VegDRI anomalies continued to become more negative during the fall and corresponded well with changes in the NLDAS modeled TC moisture content.

3.3. Crop yield analysis

In this section, we assess the impact of the severe flash drought conditions on the end-of-season yield for major agricultural crops grown across the central U.S. Fig. 6 shows the trend-adjusted yield departures for corn, soybeans, winter wheat, and spring wheat during 2012, along with ESI_4WK, NMV_AVE TC soil moisture, VegDRI, and SPI_8WK anomalies during critical times for yield production in each crop. The yield departures are expressed as percentages above and below the 2000–2014 yield trend for each county to account for local differences in average crop yield and yield trends.

Overall, it is evident that winter wheat yields were well above average across the primary wheat-growing areas in the south-central U.S., most notably in parts of western Oklahoma and eastern Kansas where yields were 50% higher than normal. Wheat yields were high in this part of the country because the warm and wet conditions during spring provided ideal growing conditions that allowed the crop to mature before severe drought conditions developed by mid-summer. Areas further to the west and north remained

in drought during the spring and early summer; thus, their yields tended to be below normal. Spring wheat yields over the northern Plains were below normal over South Dakota and Montana in areas affected by drought; however, they were slightly above normal over North Dakota where conditions were more favorable.

One of the most critical periods for wheat yield production occurs between the booting and soft dough stages during late spring for winter wheat and early summer for spring wheat (Hanks and Rasmussen, 1982). Overall, for winter wheat, there is a strong relationship between above average yield over Oklahoma and southeastern Kansas and positive ESI anomalies on 12 May, with negative ESI anomalies over the High Plains and the eastern Corn Belt where yields were below average. For spring wheat, the ESI also contains large negative anomalies in regions with below average yield, such as over most of Montana and western South Dakota. A strong correspondence also exists between the VegDRI anomalies and wheat yield departures across most of the central U.S. The NMV_AVE anomalies, however, exhibit a weaker relationship to the final yield for both crops. For example, the NMV_AVE anomalies are mostly negative across the southern Plains on 12 May where winter wheat yields were well above average but were mostly positive across Montana on 16 June where spring wheat yields were below normal.

The extreme drought conditions had a much larger impact on corn and soybean yields across the Midwest. Corn yields were below normal across most of the Corn Belt, with less than half of normal yield observed in the region extending from South Dakota southeastward across Missouri and the lower Ohio River valley. Soybean yields were also below normal in most locations, especially across the western Corn Belt and central Plains where yields

Fig. 6. Trend-adjusted yield departures (%) for 2012 for (a) winter wheat, (b) spring wheat, (c) corn, and (d) soybeans for each county computed with respect to the 2000–2014 base line period. ESI 4-wk standardized anomalies for (e) 12 May, (f) 16 June, (g) 21 July, and (h) 01 September. (i–l) Same as (e–h) except for 4-wk NMV_AVE total column soil moisture standardized anomalies. (m–p) Same as (e–h) except for VegDRI standardized anomalies. (q–t) Same as (e–h) except for 8-wk SPI standardized anomalies.

were at least 25% below the long-term trend. The different locations of the largest corn and soybean yield losses are consistent with the evolution of the most severe drought conditions during the growing season. For example, the largest corn yield reductions occurred where excessive heat in July combined with the largest precipitation deficits. July is the most important month for determining corn yield because excessive heat during that month can significantly decrease pollination efficiency during the critical silking and tasseling stages (Lobell et al., 2013; Shafiee-Jood et al., 2014). For soybeans, however, the most important development stages occur during the second half of summer when soybean pods develop and the seeds still have time to increase in size if the plants receive adequate rainfall. This meant that soybean yield losses were less severe east of the Mississippi River because of heavy rainfall during August and September, but were larger to the west as the core drought region shifted westward during the summer.

Comparison of the drought indices on 21 July reveals that the spatial pattern in the ESI anomalies most accurately corresponds to the observed corn yield departures across most of the Corn Belt, including the much below average yield from Missouri to southern Indiana and the above average yield over Minnesota and North

Dakota. The NMV_AVE anomalies were also strongly negative across the central and eastern Corn Belt; however, the large anomalies extended too far to the north into areas that actually had near to above average corn yields. Though VegDRI also exhibits negative anomalies in most locations, its correspondence to the final corn yield is much weaker than the other datasets because of its slow response to the rapidly changing conditions experienced during this drought. Its performance improved for soybeans, with negative anomalies and a spatial pattern that more closely matches those depicted by the SPI_8WK, ESI and NMV_AVE datasets during the bean filling stage (e.g. 01 September).

To further assess relationships between the various drought indices and the 2012 crop yields, correlations were computed between the county-level trend-adjusted crop yield departures and the ESI_4WK, SPI_8WK, VEGDRI, and NMV_AVE TC anomalies at weekly intervals during the growing season (Fig. 7). The drought monitoring datasets for a given week were averaged to the individual county level prior to computing the correlations. Table 1 provides a list of the states used to compute the correlations for each crop. The correlations typically increase for each crop as the growing season progresses and reach peak values near
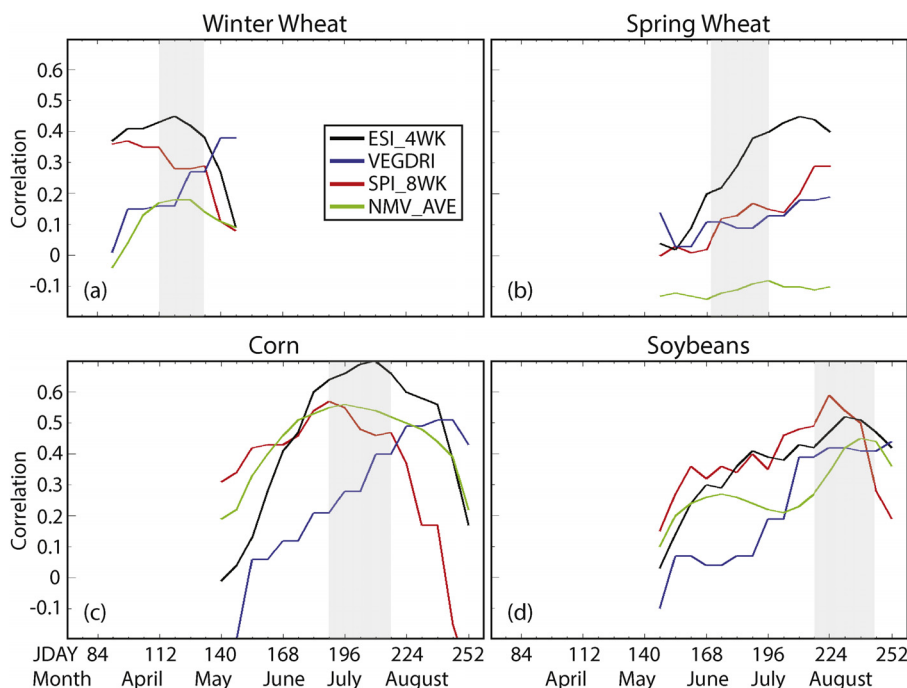
Fig. 7. Time series of correlations between county-level trend-adjusted crop yield departures (%) for (a) winter wheat, (b) spring wheat, (c) corn, and (d) soybeans and ESI_4WK (black), VEGDRI (blue), SPI_8WK (red), and NMV_AVE (green) anomalies at weekly intervals during 2012. The gray-shaded regions in each panel indicate critical development periods for each crop. The time series are only plotted during the growing season for a given crop. (For interpretation of the references to color in this figure legend, the reader is referred to the web version of this article.)

Table 1
States used to compute the yield correlations for winter wheat, spring wheat, corn, and soybeans. The correlations were computed using all counties within these states that reported crop yields during 2012.

Crop	States
Winter wheat	Colorado, Illinois, Indiana, Kansas, Kentucky, Michigan, Missouri, Montana, Nebraska, North Dakota, Ohio, Oklahoma, South Dakota, Tennessee, and Wisconsin
Spring wheat	Minnesota, Montana, North Dakota, and South Dakota
Corn	Illinois, Indiana, Iowa, Kansas, Kentucky, Michigan, Minnesota, Missouri, Nebraska, North Dakota, Ohio, South Dakota, and Wisconsin
Soybeans	Illinois, Indiana, Iowa, Kansas, Kentucky, Michigan, Minnesota, Missouri, Nebraska, North Dakota, Ohio, South Dakota, and Wisconsin

critical stages of yield development (shaded areas in Fig. 7). For most crops, the ESI_4WK data exhibited the strongest correlations to yield anomalies during these critical stages, most notably for corn, spring wheat, and winter wheat. Given the importance of rainfall for yield production, the SPI_8WK correlations were also strong, but were weaker than those computed using the ESI_4WK data except for soybeans. The stronger correlations exhibited by the ESI_4WK variable demonstrates that although rainfall departures are important for yield production, it is also necessary to consider other drivers of drought such as hot temperatures when assessing agricultural drought severity and potential impact on yield. Correlations with VEGDRI were generally weaker than the other variables during the spring and early summer due to its slow response to the rapidly changing conditions, but increased as drought conditions became entrenched across the region, with its maximum correlations obtained near the end of the growing season. Finally, although the NMV_AVE correlations were relatively strong for corn, they were weaker for the other crops and were even negative for spring wheat. Further research is necessary to determine why the modeled soil moisture anomalies had such a weak relationship to crop yields during this extreme flash drought event.

4. Conclusions and discussion

This study examined the evolution of several drought indicators sensitive to soil moisture and vegetation conditions during

the extreme flash drought event that impacted most of the U.S., including some of the world's most productive farmland, during 2012. The evolution of two satellite-based drought indicators, the ESI and VegDRI, was compared to modeled soil moisture anomalies from NLDAS and to observed soil moisture and crop conditions compiled by the USDA NASS. The modeled soil moisture anomalies were assessed separately for the Noah, Mosaic, and VIC models in the NLDAS system, and also for their ensemble mean. The response of each of these datasets was compared to observed meteorological conditions and assessed at both national and regional scales.

Overall, the results showed that rapid temporal changes in the NLDAS and ESI datasets often preceded periods of rapid drought intensification in the USDM. In most locations, dry conditions initially appeared in the NLDAS TS moisture anomalies before appearing in the ESI and NLDAS TC soil moisture anomalies in subsequent weeks. This sequence occurs because except for early in the growing season when root depths are still shallow, vegetation will be able to access soil moisture over more than just the top 10 cm of the column, which means that ET can remain high even as the TS moisture decreases. For agricultural drought detection, however, the heightened sensitivity of the TS moisture to rainfall can lead to false alarms when dry spells are short-lived. Thus, when assessing agricultural drought severity, it is advantageous to use drought indices that are sensitive to vegetation, yet able to respond quickly to changing conditions. Decreases in

the short-range (2- and 4-wk) ESI anomalies preceded observed changes in crop conditions by up to one month in the regional analyses, which is consistent with prior studies by Otkin et al. (2013, 2014). The NLDAS anomalies were typically similar to concurrent anomalies in the NASS TS and subsoil moisture datasets. The VegDRI anomalies were most similar to the TC soil moisture anomalies because that method uses longer-term climate indicators in addition to remotely sensed vegetation health estimates to assess drought severity. VegDRI anomalies tended to match the evolution of the USDM in regions with slow drought development, but lagged the USDM and other drought indicators when conditions were changing rapidly, making it less suitable as a flash drought early warning tool. For early warning during rapid onset drought events, it is important to use drought metrics that are able to capture rapid changes in precipitation, soil moisture, and vegetation conditions.

Comparison of the NLDAS soil moisture anomalies revealed large differences in behavior for each of the models assessed during this study. The Noah model consistently depicted the largest soil moisture anomalies, whereas moisture deficits in the VIC model were often less severe because of its greater sensitivity to small rainfall events. In many situations, the larger improvements depicted by the VIC model were reasonable based on changes in the NASS soil moisture datasets; however, sometimes these improvements were too large. More detailed process studies are necessary to identify the reasons for the model differences and to determine if they also occur during less extreme drought events.

A detailed assessment of the NASS crop conditions for three regions revealed that range conditions were typically the first to deteriorate as drought severity increased followed thereafter by decreases in corn and soybean conditions. Comparison to the ESI anomalies showed that soybean conditions were most similar to the short-range (2 and 4 wk) ESI composites, whereas corn conditions more closely followed changes in the longer 8- and 12-wk ESI anomalies. This behavior suggests that crop-specific drought indices could be developed using ESI anomalies computed over different time periods that are optimized to depict conditions experienced by each crop. More research is required to assess this possibility.

Crop yield departures were also assessed using county-level yield data. Winter wheat yields were generally above average because that crop matured before the most severe drought conditions developed; however, significant yield losses occurred for both corn and soybeans. Corn yield losses were largest across those regions that experienced both extreme heat and dry weather during the pollination stage in July. Soybean losses were largest across the western Corn Belt because of the extreme drought conditions that developed there during the second half of summer when seed growth occurs. These yield losses were consistent with the drought severity depicted by the ESI and SPI and to a lesser extent by the NLDAS and VegDRI datasets. These results demonstrate the utility of county-level crop information for ground truth assessment of drought indices.

Acknowledgements

References

Allen, R.G., Pereira, L.S., Raes, D., Smith, M., 1998. Crop evapotranspiration – guidelines for computing crop water requirements. FAO Irrigation and Drainage Paper No. 56. FAO, Rome.

Anderson, M.C., Norman, J.M., Diak, G.R., Kustas, W.P., Mecikalski, J.R., 1997. A two-source time-integrated model for estimating surface fluxes using thermal infrared remote sensing. Remote Sens. Environ. 60, 195–216.

Anderson, M.C., Norman, J.M., Mecikalski, J.R., Otkin, J.A., Kustas, W.P., 2007a. A climatological study of evapotranspiration and moisture stress across the continental U.S. based on thermal remote sensing: 1. Model formulation. J. Geophys. Res. 112, D10117, http://dx.doi.org/10.1029/2006JD007506.

Anderson, M.C., Norman, J.M., Mecikalski, J.R., Otkin, J.A., Kustas, W.P., 2007b. A climatological study of evapotranspiration and moisture stress across the continental U.S. based on thermal remote sensing: 2. Surface moisture climatology. J. Geophys. Res. 112, D11112, http://dx.doi.org/10.1029/2006JD007507.

Anderson, M.C., Hain, C., Wardlow, B., Pimstein, A., Mecikalski, J.R., Kustas, W.P., 2011. Evaluation of drought indices based on thermal remote sensing and evapotranspiration over the continental United States. J. Climate 24, 2025–2044.

Anderson, M.C., Hain, C., Otkin, J.A., Zhan, X., Mo, K., Svoboda, M., Wardlow, B., Pimstein, A., 2013. An intercomparison of drought indicators based on thermal remote sensing and NLDAS simulations. J. Hydrometeor. 14, 1035–1056.

Barlage, M., et al., 2010. Noah land surface model improvements to improve snowpack prediction in the Colorado Rocky Mountains. J. Geophys. Res. 115, D22101, http://dx.doi.org/10.1029/2009JD013470.

Barnabás, B., Jäger, K., Fehér, A., 2008. The effect of drought and heat stress on reproductive processes in cereals. Plant Cell Environ. 31, 11–38.

Blunden, J., Arndt, D.S., 2013. State of the climate in 2012. Bull. Am. Meteorol. Soc. 94, S1–S258.

Boyer, J.S., et al., 2013. The U.S. drought of 2012 in perspective: a call to action. Global Food Secur. 2, 139–143.

Brown, J.F., Wardlow, B.D., Tadesse, T., Hayes, M.J., Reed, B.C., 2008. The Vegetation Drought Response Index (VegDRI): a new integrated approach for monitoring drought stress in vegetation. GIScience Remote Sens. 45, 16–46.

Calvino, P.A., Andrade, F.H., Sadras, V.O., 2003. Maize yield as affected by water availability, soil depth, and crop management. Agron. J. 95, 275–281.

Diffenbaugh, N.S., Sherer, M., 2013. Likelihood of July 2012 U.S. temperatures in preindustrial and current forcing regimes. Bull. Am. Meteorol. Soc. 94, S6–S9.

Earl, H.J., Davis, R.F., 2003. Effect of drought stress on leaf and whole canopy maize radiation use efficiency and yield of maize. Agron. J. 95, 688–696.

Ek, M.B., et al., 2003. Implementation of Noah land surface model advances in the National Centers for Environmental Prediction operational mesoscale Eta model. J. Geophys. Res. 108, 8851, http://dx.doi.org/10.1029/2002JD003296.

Hanks, R.J., Rasmussen, V.P., 1982. Predicting crop production as related to plant water stress. Adv. Agron. 35, 193–215.

Higgins, R.W., Shi, W., Yarosh, E., Joyce, R., 2000. Improved United States Precipitation Quality Control System and Analysis. NCEP/Climate Prediction Center ATLAS No. 7, Camp Springs, MD, 40 pp.

Hoerling, M., Eischeid, J., Kumar, A., Leung, R., Mariotti, A., Mo, K., Schubert, S., Seager, R., 2014. Causes and predictability of the 2012 Great Plains drought. Bull. Am. Meteorol. Soc. 95, 269–282.

Hunt, E., Svoboda, M., Wardlow, B., Hubbard, K., Hayes, M.J., Arkebauer, T., 2014. Monitoring the effects of rapid onset of drought on non-irrigated maize with agronomic data and climate-based drought indices. J. Agric. For. Meteorol. 191A, 1–11, http://dx.doi.org/10.1016/j.agrformet.2014.02.001.

Kebede, H., Fisher, D.K., Young, L.D., 2012. Determination of moisture deficit and heat stress tolerance in corn using physiological measurements and a low-cost microcontroller-based monitoring system. J. Agron. Crop Sci. 198, 118–129.

Koster, R.D., Suarez, M.J., 1996. , 66 pp.

Kumar, A., Chen, M., Hoerling, M., Eischeid, J., 2013. Do extreme climate events require extreme forcings? Geophys. Res. Lett. 40, 3440–3445, http://dx.doi.org/10.1002/grl.50657.

Liang, X., Wood, E.F., Lettenmaier, D.P., 1996. Surface and soil moisture parameterization of the VIC-2L model: evaluation and modifications. Global Planet. Change 13, 195–206.

Lobell, D.B., Hammer, G.L., McLean, G., Messina, C., Roberts, M.J., 2013. The critical role of extreme heat for maize production in the United States. Nat. Climate Change 3, 497–501.

Lobell, D.B., et al., 2014. Greater sensitivity to drought accompanies maize yield increase in the U.S. Midwest. Science 344, 516–519.

Lydolph, P.E., 1964. The Russian Sukhovey. Ann. Assoc. Am. Geogr. 54, 291–309.

Mallya, G., Zhao, L., Song, X., Niyogi, D., Govindaraju, R., 2013. 2012 midwest drought in the United States. J. Hydrol. Eng., 737–745, http://dx.doi.org/10.1061/(ASCE)HE.1943-5584.0000786.

McKee, T.B., Doesken, N.J., Kleist, J.,1993. The relationship of drought frequency and duration to time scale. In: Proceedings of the Eighth Conference on Applied Climatology. American Meteorological Society, Boston, pp. 179–184.

McNaughton, K.G., Spriggs, T.W., 1986. A mixed-layer model for regional evaporation. Bound. -Layer Meteor. 74, 262–288.

Mesinger, F., et al., 2006. North American Regional Reanalysis. Bull. Am. Meteorol. Soc. 87, 343–360.

Meyer, S.J., Hubbard, K.G., Wilhite, D.A., 1993. A crop-specific drought index for corn: model development and validation. Agron. J. 85, 388–395.

Mishra, V.R., Cherkauer, K., 2010. Retrospective droughts in the crop growing season: implications to corn and soybean yield in the Midwestern United States. Agric. For. Meteorol. 150, 1030–1045.

Mo, K.C., Lettenmeier, D.P., 2015. Heat wave flash droughts in decline. Geophys. Res. Lett. 42, 2823–2829.

Mozny, M., Trnka, M., Zalud, Z., Hlavinka, P., Nekovar, J., Potop, V., Virag, M., 2012. Use of a soil moisture network for drought monitoring in the Czech Republic. Theor. Appl. Climatol. 107, 99–111.

Myneni, R.B., et al., 2002. Global products of vegetation leaf area and fraction absorbed by PAR from year of MODIS data. Remote Sens. Environ. 83, 214–231.

Norman, J.M., Kustas, W.P., Humes, K.S., 1995. A two-source approach for estimating soil and vegetation energy fluxes from observations of directional radiometric surface temperature. Agric. For. Meteorol. 77, 263–292.

Otkin, J.A., Anderson, M.C., Hain, C., Mladenova, I., Basara, J., Svoboda, M., 2013. Examining flash drought development using the thermal infrared based Evaporative Stress Index. J. Hydrometeor. 14, 1057–1074.

Otkin, J.A., Anderson, M.C., Hain, C., Svoboda, M., 2014. Examining the relationship between drought development and rapid changes in the Evaporative Stress Index. J. Hydrometeor. 15, 938–956.

Otkin, J.A., Anderson, M.C., Hain, C., Svoboda, M., 2015a. Using temporal changes in drought indices to generate probabilistic drought intensification forecasts. J. Hydrometeor. 16, 88–105.

Otkin, J.A., Shafer, M., Svoboda, M., Wardlow, B., Anderson, M.C., Hain, C., Basara, J., 2015b. Facilitating the use of drought early warning information through interactions with agricultural stakeholders. Bull. Am. Meteorol. Soc. 96, 1073–1078.

Peng, C., Deng, M., Di, L., 2014. Relationships between remote-sensing-based agricultural drought indicators and root zone soil moisture: a comparative study of Iowa. IEEE J. Sel. Top. Appl. 7, 4572–4580.

Prasad, P.V.V., Pisipati, S.R., Momcilivic, I., Ristic, Z., 2011. Independent and combined effects of high temperature and drought stress during grain filling on plant yield and chloroplast EF-Tu expression in spring wheat. J. Agron. Crop Sci. 197, 430–441.

Saha, S., et al., 2010. The NCEP climate system forecast reanalysis. Bull. Am. Meteorol. Soc. 91, 1015–1057.

Shafiee-Jood, M., Cai, X., Chen, L., Liang, X.-Z., Kumar, P., 2014. Assessing the value of seasonal climate forecast information through an end-to-end forecasting framework: application to U.S. 2012 drought in central Illinois. Water Resour. Res. 50, 6592–6609.

Saini, H.S., Westgate, M.E., 1999. Reproductive development in grain crops during drought. Adv. Agron. 68, 59–96.

Svoboda, M., et al., 2002. The drought monitor. Bull. Am. Meteorol. Soc. 83, 1181–1190.

Tadesse, T., et al., 2015. Assessing the vegetation condition impacts of the 2011 drought across the U.S. Southern Great Plains using the Vegetation Drought Response Index (VegDRI). J. Appl. Meteorol. Climatol. 54, 153–169.

USDA, 2012. Cattle inventory report. USDA Doc, 13 pp. Available at: http://usda01.library.cornell.edu/usda/nass/Catt/l2010s/2012/Catt-01-27-2012.pdf.

USDA, 2013. Crop production 2012 summary. USDA Doc, 95 pp. Available at: http://usda01.library.cornell.edu/usda/nass/CropProdSu/2010s/2013/CropProdSu-01-11-2013.pdf.

Wang, H., Schubert, S., Koster, R., Ham, Y.-G., Suarez, M., 2014. On the role of SST forcing in the 2011 and 2012 Extreme U.S. Heat and Drought: A study in contrasts. J. Hydrometeor. 15, 1255–1273.

Wei, H., Xia, Y., Mitchell, K.E., Ek, M.B., 2013. Improvement of the Noah land surface model for warm season processes: evaluation of water and energy flux simulation. Hydrol. Processes 27, 297–303, http://dx.doi.org/10.1002/hyp.9214.

Wells, N., Goddard, S., Hayes, M.J., 2004. A self-calibrating Palmer drought severity index. J. Climate 17, 2335–2351.

Xia, Y., Ek, M.B., Wei, H., Meng, J., 2012a. Comparative analysis of relationships between NLDAS-2 forcings and model outputs. Hydrol. Processes 26, 467–474.

Xia, Y., et al., 2012b. Continental-scale water and energy flux analysis and validation of the North American Land Data Assimilation System project phase 2 (NLDAS-2): 1. Intercomparison and application of model products. J. Geophys. Res. 117.

Xia, Y., Sheffield, J., Ek, M.B., Dong, J., Chaney, N., Wei, H., Meng, J., Wood, E.F., 2014. Evaluation of multi-model simulated soil moisture in NLDAS-2. J. Hydrol. 512, 107–125, http://dx.doi.org/10.1016/j.jhydrol.2014.02.027.